Distributed Collaborative Beamforming for Real-World WSN Applications

Slim Zaidi(✉), Bouthaina Hmidet, and Sofiène Affes

INRS-EMT, Université du Québec, Montreal, QC H5A 1K6, Canada
{zaidi,hmidet,affes}@emt.inrs.ca

Abstract. In this paper, we consider a collaborative beamformer (CB) design that achieves a dual-hop communication from a source to a receiver in highly-scattered environments, through a wireless sensor network (WSN) comprised of K independent and autonomous sensor nodes. The weights of the considered CB design at these nodes, derived to maximize the received signal-to-noise ratio (SNR) subject to constraint over the nodes total transmit power, have expressions that inevitably depend on some form of the channel state information (CSI). Only those requiring the local CSI (LCSI) available at their respective nodes lend themselves to a truly distributed implementation. The latter has the colossal advantage of significantly minimizing the huge overhead resulting otherwise from non-local CSI (NLCSI) exchange required between nodes, which becomes prohibitive for large K and/or high Doppler. We derive the closed-form expression of the SNR-optimal CB (OCB) and verify that it is a NLCSI-based design. Exploiting, however, the polychromatic (i.e., multi-ray) structure of scattered channels as a superposition of L impinging rays or chromatics, we propose a novel LCSI-based distributed CB (DCB) design that requires a minimum overhead cost and, further, performs nearly as well as its NLCSI-based OCB counterpart. Furthermore, we prove that the proposed LCSI-based DCB outperforms two other DCB benchmarks: the monochromatic (i.e., single-ray) DCB and the bichromatic (i.e., two-ray) DCB (B-DCB).

Keywords: Distributed collaborative beamforming (CB, DCB) · Relaying · MIMO · Scattering · Device/machine-2-device/machine (D2D/M2M) communications · Wireless sensor networks (WSN)

1 Introduction

Due to its strong potential in establishing a reliable and energy-efficient communication in wireless sensor networks (WSN) applications, collaborative beamforming (CB) has garnered the attention of the research community [1–12]. The so far proposed CB designs could be broadly categorized as either the local

Work supported by the CRD, DG, and CREATE PERSWADE <www.create-perswade.ca> Programs of NSERC and a Discovery Accelerator Supplement Award from NSERC.

Y. Zhou and T. Kunz (Eds.): ADHOCNETS 2016, LNICST 184, pp. 316–329, 2017.
DOI: 10.1007/978-3-319-51204-4_26

CSI (LCSI)-based (i.e., distributed) CB namely the monochromatic DCB (M-DCB) and the bichromatic DCB (B-DCB), or the non-local CSI (NLCSI)-based (i.e., non-distributed) CB namely the optimal CB. When designing M-DCB, authors in [1–12] ignored scattering present in almost all real-world scenarios but very few ones with both practical and investigation values in which they have consequently assumed a simple monochromatic (i.e., single-ray) channel. In scattered channels, however, said to be polychromatic (i.e., multi-ray) and characterized by the angular spread (AS) [13–17], due to channel mismatch, the performance of M-DCB slightly deteriorates in areas where the AS is small and becomes unsatisfactory when it grows large [18–23]. In contrast, B-DCB in [22,23] which accounts for scattering by an efficient two-ray approximation of the polychromatic channel at relatively low AS not only outperforms M-DCB, but also achieves the optimal performance at small to moderate AS values in lightly- to moderately-scattered environments. Nevertheless, its performance substantially deteriorates at large in highly-scattered environments [22,23]. OCB which is able to achieve optimal performance even in highly-scattered environments is NLCSI-based and cannot be implemented in WSNs due to its distributed nature [24]. Indeed, the often independent and autonomous sensors must estimate and broadcast their own channels at the expense of an overhead that becomes prohibitive for a large number of nodes and/or high Doppler [24,25]. The aim of this work is then to design a novel DCB technique implementation that requires a minimum overhead cost and, further, is able to achieve optimal performance for any AS values, thereby pushing farther the frontier of the DCB's real-world applicability range to include highly-scattered environments.

In this paper, we consider an OCB design whose weights are derived to maximize the received SNR subject to constraint over the nodes' total transmit power, to achieve a dual-hop communication from a source to a receiver in highly-scattered environments, through a WSN comprised of K independent and autonomous sensor nodes. We verify that the direct implementation of the so-obtained OCB is NLCSI-based. Exploiting, the polychromatic structure of scattered channels, we propose a novel DCB LCSI-based implementation that requires a minimum overhead cost and, further, performs nearly as well as its NLCSI-based OCB counterpart. Furthermore, we prove that the proposed LCSI-based DCB always outperforms M-DCB which is designed without accounting for scattering and that it is more robust against scattering than B-DCB whose performance substantially deteriorates in highly-scattered environments.

The rest of this paper is organized as follows. The system model is described in Sect. 2. Section 3 derives the power-constrained SNR-optimal CB design in closed-form and verifies that its direct implementation is NLCSI-based. Our novel DCB implementation is proposed in Sect. 4. Section 5 analyzes its performance while Sect. 6 verifies by computer simulations the theoretical results. Concluding remarks are given in Sect. 7.

Notation: Uppercase and lowercase bold letters denote matrices and column vectors, respectively. $[\cdot]_{il}$ and $[\cdot]_i$ are the (i,l)-th entry of a matrix and i-th entry of a vector, respectively. $\mathbf{I}_N$ is the N-by-N identity matrix. $(\cdot)^T$ and $(\cdot)^H$ denote

the transpose and the Hermitian transpose, respectively. $\|\cdot\|$ is the 2-norm of a vector and $|\cdot|$ is the absolute value. $\mathrm{E}\{\cdot\}$ stands for the statistical expectation and $(\xrightarrow{ep1})$ $\xrightarrow{p1}$ denotes (element-wise) convergence with probability one. $J_1(\cdot)$ is the first-order Bessel function of the first kind, $\mathrm{Ei}(\cdot)$ is the exponential integral function, and $\odot$ is the element-wise vector product.

2 System Model

Consider a WSN comprised of K single-antenna sensor nodes uniformly and independently distributed on the disc $D(O,R)$. A source S and a receiver Rx are located in the same plane containing $D(O,R)$, as illustrated in Fig. 1. Due to high pathloss attenuation, we assume that there is no direct link from S to Rx. Let (r_k,ψ_k) denote the polar coordinates of the k-th node and (A_s,ϕ_s) denote those of the source. The latter is assumed, without loss of generality, to be at $\phi_s=0$ and to be located relatively far from the nodes, i.e., $A_s \gg R$.

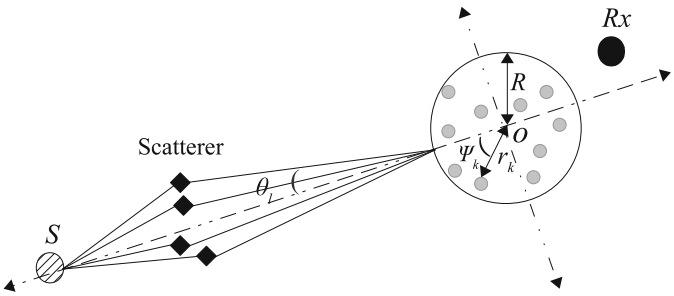

Fig. 1. System model.

Furthermore, the following assumptions are considered throughout the paper:

(A1) The source is scattered by a given number of scatterers located in the same plane containing $D(O,R)$. The latters generate from the transmit signal L rays or "spatial chromatics" (with reference to their angular distribution) that form a polychromatic propagation channel [15–18]. The l-th ray or chromatic is characterized by its angle deviation θ_l from the source direction ϕ_s and its complex amplitude $\alpha_l=\rho_l e^{j\varphi_l}$ where the amplitudes $\rho_l,\ l=1,\ldots,L$ and the phases $\varphi_l,\ l=1,\ldots,L$ are independent and identically distributed (i.i.d.) random variables, and each phase is uniformly distributed over $[-\pi,\pi]$. The $\theta_l,\ l=1,\ldots,L$ are i.i.d. zero-mean random variables with a symmetric probability density function (pdf) $p(\theta)$ and variance σ_θ^2 [13,15,16]. All θ_ls, φ_ls, and ρ_ls are mutually independent. All rays have equal power $1/L$ (i.e., $\mathrm{E}\left\{|\alpha_l|^2\right\}=1/L$). Note that the standard deviation σ_θ is commonly known as the angular spread (AS) while $p(\theta)$ is called the scattering or angular distribution. We are particularly interested here in addressing highly-scattered environments.

(A2) The nodes' forward channels to the receiver $[\mathbf{f}]_k,\ k=1,\ldots,K$ are zero-mean unit-variance circular Gaussian random variables [9,11].

(A3) The source signal s is narrow-band with unit power while noises at the nodes and the receiver are zero-mean Gaussian random variables with variances ${\sigma_v}^2$ and ${\sigma_n}^2$, respectively. The source signal, noises, and the nodes' forward channels are mutually independent [9,11,12,26].

(A4) The k-th node is aware of its own coordinates (r_k, ψ_k), its forward channel $[\mathbf{f}]_k$, its backward channel $[\mathbf{g}]_k$, and the wavelength λ while being oblivious to the locations and the forward channels of *all* other nodes in the network [1–5,11,12].

Due to A1 and the fact that $A_s \gg R$, it can be shown that the backward channel gain from the source to the k-th node can be represented as

$$[\mathbf{g}]_k = \sum_{l=1}^{L} \alpha_l e^{-j\frac{2\pi}{\lambda} r_k \cos(\theta_l - \psi_k)}. \tag{1}$$

Obviously, in the conventional scenario where the scattering effect is neglected (i.e., $\sigma_\theta \longrightarrow 0$) to assume a monochromatic plane-wave propagation channel, we have $\theta_l = 0$ and, hence, $[\mathbf{g}]_k$ can be reduced to $[\mathbf{g}_1]_k = e^{-j(2\pi/\lambda) r_k \cos(\psi_k)}$, the well-known steering vector in the array-processing literature [1–12,19–25].

As can be observed from (1), the summation of L chromatics causes a variation, with a particular channel realization, of the received power at the k-th node. The channel is then said to experience a form of fading. When L is large, according to the Central Limit Theorem, the distribution of the channel gain $[\mathbf{g}]_k$ approaches a Gaussian. Since, according to A1, $\mathrm{E}\{\alpha_l\} = 0$ for $l = 1, \ldots, L$, then $[\mathbf{g}]_k$ is a zero-mean Gaussian random variable and, hence, its magnitude is Rayleigh distributed. Therefore, when L is large enough (practically in the range of 10), the channel from the source to the k-th node is nothing but a Rayleigh channel. It can also be observed from (1) that we did not take into account any line-of-sight (LOS) component in our channel model. If this were the case, $[\mathbf{g}]_k$'s distribution would approach a non-zero mean Gaussian distribution and the channel would become Rician.

A dual-hop communication is established from the source S to the receiver Rx. In the first time slot, S sends its signal s to the nodes while, in the second time slot, each node multiplies its received signal by a properly selected beamforming weight and forwards the resulting signal Rx. The received signal at the latter is given by

$$r = s\mathbf{w}^H\mathbf{h} + \mathbf{w}^H(\mathbf{f} \odot \mathbf{v}) + n, \tag{2}$$

where $\mathbf{w} \triangleq [w_1 \ldots w_K]$ is the beamforming vector with w_k being the k-th node's beamforming weight, $\mathbf{h} \triangleq \mathbf{f} \odot \mathbf{g}$ with $\mathbf{f} \triangleq [[\mathbf{f}]_1 \ldots [\mathbf{f}]_K]^T$ and $\mathbf{g} \triangleq [[\mathbf{g}]_1 \ldots [\mathbf{g}]_K]^T$, and $\mathbf{v}$ and n are the nodes' noise vector and the receiver noise, respectively. Several CB designs exist in the literature but we are only concerned herein by the one which maximizes the received signal-to-noise ratio (SNR) subject to constraint over the nodes' total transmit power [26].

3 Power-Constrained SNR-Optimal CB

Let $\mathbf{w}_{\mathrm{O}}$ denote the power-constrained SNR-optimal CB, or simply OCB, which satisfies the following optimization problem:

$$\mathbf{w}_{\mathrm{O}} = \arg\max \xi_{\mathbf{w}} \quad \text{s.t.} \quad P_{\mathrm{T}} \leq P_{\max}, \tag{3}$$

where $\xi_{\mathbf{w}}$ is the achieved SNR using $\mathbf{w}$ and $P_{\mathrm{T}} = (1+\sigma_v^2)\left\|\mathbf{w}\right\|^2$ is the nodes' total transmit power. From (2), $\xi_{\mathbf{w}}$ is given by

$$\xi_{\mathbf{w}} = \frac{P_{\mathbf{w},s}}{P_{\mathbf{w},n}}, \tag{4}$$

where $P_{\mathbf{w},s} = |\mathbf{w}^H\mathbf{h}|^2$ and $/P_{\mathbf{w},n} = \sigma_v^2\mathbf{w}^H\mathbf{\Lambda}\mathbf{w} + \sigma_n^2$ are, respectively, the desired and noise powers with $\mathbf{\Lambda} \triangleq \mathrm{diag}\{|[\mathbf{f}]_1|^2 \ldots |[\mathbf{f}]_K|^2\}$. Note that $\mathbf{w}_{\mathrm{O}}$ should satisfy the constraint in (3) with equality. Otherwise, one could find $\epsilon > 1$ such that $\mathbf{w}_\epsilon = \epsilon\mathbf{w}_{\mathrm{O}}$ verifies $(1+\sigma_v^2)\left\|\mathbf{w}_\epsilon\right\|^2 = P_{\max}$. In such a case, since $d\xi_{\mathbf{w}_\epsilon}/d\epsilon > 0$ for any $\epsilon > 0$, the SNR achieved by $\mathbf{w}_\epsilon$ would be higher than that achieved by $\mathbf{w}_{\mathrm{O}}$ contradicting thereby the optimality of the latter. As such, (3) could be rewritten as

$$\mathbf{w}_{\mathrm{O}} = \arg\max \frac{\mathbf{w}^H\mathbf{h}\mathbf{h}^H\mathbf{w}}{\sigma_v^2\mathbf{w}^H\tilde{\mathbf{\Lambda}}\mathbf{w}} \quad \text{s.t.} \quad (1+\sigma_v^2)\left\|\mathbf{w}\right\|^2 = P_{\max}, \tag{5}$$

where $\tilde{\mathbf{\Lambda}} = \mathbf{\Lambda} + \beta\mathbf{I}$ and $\beta = \sigma_n^2(1+\sigma_v^2)/\left(\sigma_v^2 P_{\max}\right)$. It is straightforward to show that the OCB solution of (5) is

$$\mathbf{w}_{\mathrm{O}} = \left(\frac{P_{\max}}{K\left(1+\sigma_v^2\right)\eta}\right)^{\frac{1}{2}} \tilde{\mathbf{\Lambda}}^{-1}\mathbf{h}, \tag{6}$$

where $\eta = \left(\mathbf{h}^H\tilde{\mathbf{\Lambda}}^{-2}\mathbf{h}\right)/K$. Nevertheless, according to (6), OCB is a NLCSI-based design since the computation of its beamforming weight $[\mathbf{w}_{\mathrm{O}}]_k$ at the k-th node depends on information unavailable locally, namely $[\mathbf{g}]_k,\ k = 1, \ldots, K$ and $[\mathbf{f}]_k,\ k = 1, \ldots, K$ as well as $P_{\max}/K$ and $\sigma_n^2/P_{\max}$. In order to implement $\mathbf{w}_{\mathrm{O}}$ in the considered WSN, each node should then estimate its backward channel and broadcast it over the network along with its forward channel. This process results in an undesired overhead which becomes prohibitive especially for large K and/or high backward channel's Doppler, resulting thereby in substantial throughput losses [24]. Therefore, OCB is unsuitable for implementation in WSNs, unless relatively exhaustive overhead exchange over the air were acceptable or if $\mathbf{w}_{\mathrm{O}}$ were to be implemented in conventional beamforming, i.e., over a unique physical terminal that connects to a K-dimensional distributed antenna system (DAS).

4 Proposed DCB Implementation

In order to reduce the excessively large implementation overhead incurred by the NLCSI-based OCB, we resort to substitute η with a quantity that could be

locally computed by all nodes at a negligible overhead cost. This quantity must also well-approximate η to preserve the optimality of the solution in (6). In this paper, we propose to use $\eta_{\mathrm{D}} = \lim_{K\to\infty} \eta$ in lieu of η. First, we show that

$$\eta = \frac{1}{K}\sum_{k=1}^{K} \frac{|[\mathbf{f}]_k|^2}{\left(|[\mathbf{f}]_k|^2+\beta\right)^2} \sum_{l=1}^{L}\sum_{m=1}^{L} \alpha_l \alpha_m^* e^{j4\pi \sin\left(\frac{\theta_l-\theta_m}{2}\right) z_k}, \tag{7}$$

where $z_k = (r_k/\lambda)\sin\left((\theta_l+\theta_m)/2 - \psi_k\right)$. Using the strong law of large numbers and the fact that r_k, ψ_k and $[\mathbf{f}]_k$ are all mutually statistically independent, we have

$$\eta_{\mathrm{D}} = \lim_{K\to\infty} \eta \xrightarrow{p1} \rho_1 \sum_{l=1}^{L}\sum_{m=1}^{L} \alpha_l \alpha_m^* \Delta\left(\theta_l - \theta_m\right), \tag{8}$$

where $\rho_1 = \mathrm{E}\left\{|[\mathbf{f}]_k|^2/\left(|[\mathbf{f}]_k|^2+\beta\right)^2\right\} = -(1+\beta)e^{\beta}\mathrm{Ei}(-\beta) - 1$ and $\Delta(\phi) = \mathrm{E}\left\{e^{j4\pi\sin(\phi/2)z_k}\right\}$. Note that to derive the closed-form expression of $\Delta(\phi)$, the z_k's pdf $f_{z_k}(z)$ which is closely related to the nodes' spatial distribution is required. In this paper, we are only concerned by the main distributions frequently used in the context of collaborative beamforming that are: Uniform distribution and Gaussian distribution. It can be shown that [1,2]

$$f_{z_k} = \begin{cases} \frac{2\lambda}{R\pi}\sqrt{1-\left(\frac{\lambda}{R}z\right)^2}, & -\frac{R}{\lambda} \le z \le \frac{R}{\lambda} \quad \text{Uniform} \\ \frac{\lambda}{\sqrt{2\pi}\sigma} e^{-\frac{(\lambda z)^2}{2\sigma^2}}, & -\infty \le z \le \infty \quad \text{Gaussian} \end{cases}, \tag{9}$$

where σ^2 random variables corresponding to the nodes' cartesian coordinates. Using (9) we obtain

$$\Delta(\phi) = \begin{cases} 2\frac{J_1\left(4\pi\frac{R}{\lambda}\sin(\phi/2)\right)}{4\pi\frac{R}{\lambda}\sin(\phi/2)}, & \phi \neq 0 \quad \text{Uniform} \\ 1, & \phi = 0 \\ e^{-8\left(\pi\frac{\sigma}{\lambda}\sin(\phi/2)\right)^2}, & \text{Gaussian} \end{cases}. \tag{10}$$

Substituting η with η_{D} in (6), we introduce

$$\mathbf{w}_{\mathrm{P}} = \left(\frac{P_{\max}}{K\left(1+\sigma_v^2\right)\eta_{\mathrm{D}}}\right)^{\frac{1}{2}} \tilde{\mathbf{\Lambda}}^{-1}\mathbf{h}, \tag{11}$$

the beamforming vector of our proposed DCB. From (11), in contrast with $[\mathbf{w}_{\mathrm{O}}]_k$, the k-th node's beamforming weight $[\mathbf{w}_{\mathrm{P}}]_k$ solely depends on the forward and backward channels $[\mathbf{f}]_k$ and $[\mathbf{g}]_k$, respectively, which can be locally estimated. Therefore, according to (11), the proposed beamformer is a LCSI-based design that requires only a negligible overhead that does not grow neither with K nor with the Doppler, namely $P_{\max}/K$, $\sigma_n^2/P_{\max}$, and R or σ depending on the

nodes' spatial distribution. Consequently, the proposed LCSI-based DCB is much more suitable for a distributed implementation over WSN than its NLCSI-based OCB counterpart. Furthermore, we will prove in the sequel that it performs nearly as well as the latter even for a relatively small number of nodes. We will also compare it with two other LCSI-based DCB benchmarks, namely M-DCB and the recently developed B-DCB. The former's design ignores scattering and assumes a monochromatic channel and, hence, its CB solution reduces from (11) to

$$\mathbf{w}_{\mathrm{M}} = \left(\frac{P_{\max}}{K\left(1+\sigma_v^2\right)\rho_1}\right)^{\frac{1}{2}} \tilde{\mathbf{\Lambda}}^{-1}\mathbf{a}(0), \tag{12}$$

where $\mathbf{a}(\phi) \triangleq \left[[\mathbf{a}(\theta)]_1 \ldots [\mathbf{a}(\theta)]_K\right]^T$ with $[\mathbf{a}(\theta)]_k = [\mathbf{f}]_k e^{-j(2\pi/\lambda)r_k\cos(\theta-\psi_k)}$. In turn, the B-DCB design whose CB solution is given by

$$\mathbf{w}_{\mathrm{BD}} = \left(\frac{P_{\max}}{K\left(1+\sigma_v^2\right)\rho_1}\right)^{\frac{1}{2}} \frac{\tilde{\mathbf{\Lambda}}^{-1}\left(\mathbf{a}(\sigma_\theta)+\mathbf{a}(-\sigma_\theta)\right)}{\left(1+\Delta\left(2\sigma_\theta\right)\right)}, \tag{13}$$

relies on a polychromatic channel's approximation by two chromatics at $\pm\sigma_\theta$ when the latter is relatively small. Note that from (12) and (13) both $\mathbf{w}_{\mathrm{M}}$ and $\mathbf{w}_{\mathrm{BD}}$ depends on the information commonly available at each node and, hence, are also suitable for a distributed implementation in WSNs.

5 Performance Analysis of the Proposed DCB

Let $\bar{\xi}_{\mathbf{w}} = \mathrm{E}\left\{P_{\mathbf{w},s}/P_{\mathbf{w},n}\right\}$ be the achieved average SNR (ASNR) using the CB vector $\mathbf{w}$. Note that the expectation is taken with respect to r_k, ψ_k and $[\mathbf{f}]_k$ for $k = 1, \ldots, K$ and α_l and θ_l for $l = 1, \ldots, L$. Since to the best of our knowledge, $\bar{\xi}_{\mathbf{w}}$ for $\mathbf{w} \in \{\mathbf{w}_{\mathrm{P}}, \mathbf{w}_{\mathrm{O}}, \mathbf{w}_{\mathrm{M}}\}$ is untractable in closed-form thereby hampering a its study rigorously, we propose to adopt the average-signal-to-average-noise ratio (ASANR) $\tilde{\xi}_{\mathbf{w}} = \mathrm{E}\left\{P_{\mathbf{w},s}\right\}/\mathrm{E}\left\{P_{\mathbf{w},n}\right\}$ as a performance measure instead to gauge the proposed DCB against its benchmarks.

5.1 Proposed DCB vs M-DCB

Following derivation steps similar to those in [22, Appendix A] and exploiting the fact that, according to A1, we have

$$\mathrm{E}\left\{\alpha_l^*\alpha_m\right\} = \begin{cases} 0 & l \neq m \\ \frac{1}{L} & l = m \end{cases}, \tag{14}$$

we obtain $\mathrm{E}\left\{P_{\mathbf{w}_{\mathrm{P}},s}\right\} = \frac{P_{\max}}{(1+\sigma_v^2)\rho_1}\left(\rho_2 + (K-1)\rho_3^2\right)$ where $\rho_2 = \mathrm{E}\{|[\mathbf{f}]_k|^4/(|[\mathbf{f}]_k|^2+\beta)^2\} = 1+\beta+\beta(2+\beta)e^{\beta}\mathrm{Ei}(-\beta)$ and $\rho_3 = \mathrm{E}\left\{|[\mathbf{f}]_k|^2/\left(|[\mathbf{f}]_k|^2+\beta\right)\right\} = 1+\beta e^{\beta}\mathrm{Ei}(-\beta)$. Furthermore, to derive $\mathrm{E}\left\{P_{\mathbf{w}_{\mathrm{P}},n}\right\}$, one must first take the expectation only over the r_ks, ψ_ks and $[\mathbf{f}]_k$s yielding to

$$\mathrm{E}\left\{P_{\mathbf{w}_\mathrm{P},n}\right\} = \mathrm{E}_{\alpha_l,\theta_l}\left\{\frac{\sigma_v^2 P_{\max}\rho_2 \sum_{l,m=1}^{L}\alpha_l\alpha_m^*\Delta\left(\theta_l-\theta_m\right)}{\left(1+\sigma_v^2\right)\eta_\mathrm{D}}\right\} + \sigma_n^2$$
$$= \sigma_v^2\frac{P_{\max}\rho_2}{\left(1+\sigma_v^2\right)\rho_1} + \sigma_n^2. \tag{15}$$

It directly follows from the latter results that the achieved ASANR using the proposed DCB is

$$\tilde{\xi}_{\mathbf{w}_\mathrm{P}} = \frac{\rho_2 + (K-1)\rho_3^2}{\sigma_v^2\left(\rho_2+\beta\rho_1\right)}. \tag{16}$$

As can be observed from (16), $\tilde{\xi}_{\mathbf{w}_\mathrm{P}}$ linearly increases with the number of nodes K. More importantly, from the latter result, $\tilde{\xi}_{\mathbf{w}_\mathrm{P}}$ does not depend on the AS σ_θ meaning that the proposed DCB's performance is not affected by the scattering phenomenon even in highly-scattered environments where σ_θ is large.

Now, let us focus on the achieved ASANR $\tilde{\xi}_{\mathbf{w}_\mathrm{M}}$ using M-DCB. Following the same approach above, one can prove that

$$\tilde{\xi}_{\mathbf{w}_\mathrm{M}} = \frac{\rho_2 + (K-1)\rho_3^2\int_\Theta p(\theta)\Delta^2(\theta)\,d\theta}{\sigma_v^2\left(\rho_2+\beta\rho_1\right)}, \tag{17}$$

where Θ is the span of the pdf $p(\theta)$ over which the integral is calculated[1]. Since $\Delta(0) = 1$ regardless of the nodes spatial distribution, it follows from (16) and (17) that when there is no scattering (i.e., $\sigma_\theta = 0$), $\tilde{\xi}_{\mathbf{w}_\mathrm{M}} = \tilde{\xi}_{\mathbf{w}_\mathrm{P}}$. In such a case, indeed, $\mathbf{w}_\mathrm{P} = \mathbf{w}_\mathrm{M}\sum_{l=1}\alpha_l/\sqrt{\sum_{l=1}\alpha_l\sum_{m=1}\alpha_m^*}$ and, hence, $P_{\mathbf{w}_\mathrm{P},s} = P_{\mathbf{w}_\mathrm{M},s}\sum_{l=1}\alpha_l\sum_{m=1}\alpha_m^*$. Since according to (14) $\mathrm{E}\{\sum_{l=1}\alpha_l\sum_{m=1}\alpha_m^*\} = 1$, we have $\mathrm{E}\{P_{\mathbf{w}_\mathrm{P},s}\} = \mathrm{E}\{P_{\mathbf{w}_\mathrm{M},s}\}$. Furthermore, it is straightforward to show that $P_{\mathbf{w}_\mathrm{P},n} = P_{\mathbf{w}_\mathrm{M},n}$ when $\sigma_\theta = 0$ and, therefore, M-DCB achieves the same ASANR as the proposed DCB when there is no scattering. This is in fact expected since the assumption of monochromatic channel made when designing the monochromatic solution is valid in such a case. Nevertheless, assuming that the nodes's spatial distribution and the scattering distribution $p(\theta)$ are both Uniform, it can be shown for relatively small AS that [27]

$$\tilde{\xi}_{\mathbf{w}_\mathrm{M}} \simeq \frac{\rho_2 + (K-1)\rho_3^2 {}_3F_4\left(\frac{1}{2},2,\frac{3}{2};\frac{3}{2},2,2,3,-12\pi^2\left(\frac{R}{\lambda}\right)^2\sigma_\theta^2\right)}{\sigma_v^2\left(\rho_2+\beta\rho_1\right)}, \tag{18}$$

where ${}_3F_4\left(\frac{1}{2},2,\frac{3}{2};\frac{3}{2},2,2,3,-12\pi^2(R/\lambda)^2x^2\right)$ is a decreasing function of x whose peak is reached at 0 known as hypergeometric function. It can be inferred from (18), that the ASANR achieved by the M-DCB decreases when the AS σ_θ and/or R/λ increases. This is in contrast with the proposed DCB whose ASANR remains constant for any σ_θ and R/λ. Therefore, the proposed DCB is more robust against scattering than M-DCB whose design ignores the presence of scattering thereby resulting in a channel mismatch that causes severe ASANR deterioration.

[1] In the Gaussian and Uniform distribution cases, $\Theta = [-\inf, +\inf]$ and $\Theta = [-\sqrt{3}\sigma_\theta, +\sqrt{3}\sigma_\theta]$, respectively.

5.2 Proposed DCB vs B-DCB

It can be shown that the achieved ASANR using B-DCB is given by [22]

$$\tilde{\xi}_{\mathbf{w}_{\mathrm{BD}}} = \frac{2\rho_2 + \frac{(K-1)\rho_3^2}{(1+\Delta(2\sigma_\theta))} \int_\Theta p(\theta) \left(\Delta(\theta+\sigma_\theta) + \Delta(\theta-\sigma_\theta)\right)^2 d\theta}{\sigma_v^2 \left(\rho_2 + \beta\rho_1\right)\left(1+\Delta(2\sigma_\theta)\right)}. \tag{19}$$

It follows from (19) that when there is no scattering (i.e., $\sigma_\theta = 0$), $\tilde{\xi}_{\mathbf{w}_{\mathrm{BD}}}$ boils down as expected to its maximum level $\tilde{\xi}_{\mathbf{w}_{\mathrm{P}}}$, regardless the nodes spatial distribution. Since, as has been shown in [22,23], B-DCB is able to achieve its maximum ASANR level for small to moderate AS values such as in lightly- to moderately-scattered environments, it turns out that the proposed DCB and its B-DCB counterpart achieve the same ASANR in such environments. However, when σ_θ is large such as in highly-scattered environments, using the fact that $\Delta(2\sigma_\theta) \simeq 0$ for large σ_θ, one can easily show that $\lim_{K\to\infty} \tilde{\xi}_{\mathbf{w}_{\mathrm{BD}}}/\tilde{\xi}_{\mathbf{w}_{\mathrm{P}}} = \int_\Theta p(\theta) \left(\Delta(\theta+\sigma_\theta) + \Delta(\theta-\sigma_\theta)\right)^2 d\theta$. Since the right-hand side (RHS) of the latter equality is a decreasing function of σ_θ, the ASANR gain achieved by the proposed DCB against B-DCB increases with the latter. Consequently, in highly-scattered environments where the AS is large, the proposed DCB outperforms B-DCB whose performance deteriorates due to the channel mismatch.

5.3 Proposed DCB vs OCB

As $P_{\mathbf{w}_{\mathrm{O}},s}$ and $P_{\mathbf{w}_{\mathrm{O}},n}$ are a very complicated functions of several random valuables, it turns out that it is impossible to derive the ASANR $\tilde{\xi}_{\mathbf{w}_{\mathrm{O}}}$ in closed-form. However, a very interesting result could be obtained for large K. Indeed, one can show that

$$\begin{aligned}\lim_{K\to\infty} \frac{\tilde{\xi}_{\mathbf{w}_{\mathrm{O}}}}{\tilde{\xi}_{\mathbf{w}_{\mathrm{P}}}} &= \frac{\left(\rho_2+\beta\rho_1\right) \mathrm{E}\left\{\frac{1}{\eta_{\mathrm{D}}}\left(\lim_{K\to\infty} \frac{\mathbf{h}^H\tilde{\mathbf{\Lambda}}^{-1}\mathbf{h}}{K}\right)^2\right\}}{\rho_3^2\left(\mathrm{E}\left\{\frac{1}{\eta_{\mathrm{D}}} \lim_{K\to\infty} \frac{\mathbf{h}^H\tilde{\mathbf{\Lambda}}^{-1}\mathbf{\Lambda}\tilde{\mathbf{\Lambda}}^{-1}\mathbf{h}}{K}\right\} + \beta\right)} \\ &\xrightarrow{p1} \frac{\frac{(\rho_2+\beta\rho_1)}{\rho_1}\mathrm{E}\left\{\left(\sum_{l,m=1}^{L} \alpha_l\alpha_m^* \Delta(\theta_l-\theta_m)\right)\right\}}{\frac{\rho_2}{\rho_1}+\beta} = 1,\end{aligned} \tag{20}$$

where the third line exploits (14) while the second exploits the law of large numbers by which we can prove that $\lim_{K\to\infty} \mathbf{h}^H\tilde{\mathbf{\Lambda}}^{-1}\mathbf{h}/K = \rho_3 \sum_{l,m=1}^{L} \alpha_l\alpha_m^* \Delta(\theta_l-\theta_m)$ and $\lim_{K\to\infty} \mathbf{h}^H\tilde{\mathbf{\Lambda}}^{-1}\mathbf{\Lambda}\tilde{\mathbf{\Lambda}}^{-1}\mathbf{h}/K = \rho_2 \sum_{l,m=1}^{L} \alpha_l\alpha_m^* \Delta(\theta_l-\theta_m)$. For large K, the latter result proves that the proposed LCSI-based DCB is able to achieve the same ASANR as the NLCSI-based OCB and, therefore, is able to reach optimality for any AS value. This further proves the efficiency of the proposed DCB.

Using the same method as in (20), one can easily show that $\lim_{K\to\infty} \tilde{\xi}_{\mathbf{w}}/\bar{\xi}_{\mathbf{w}} \xrightarrow{p1} 1$ for $\mathbf{w} \in \{\mathbf{w}_{\mathrm{P}}, \mathbf{w}_{\mathrm{O}}, \mathbf{w}_{\mathrm{M}}\}$. Therefore, all the above results hold also for the ASNR as K grows large.

6 Simulation Results

All the empirical average quantities, in this section, are obtained by averaging over 10^6 random realizations of all random variables. In all simulations, the number of rays or chromatics is $L = 10$ and the noises' powers σ_n^2 and σ_v^2 are 10 dB below the source transmit power $p_s = 1$ power unit on a relative scale. We also assume that the scattering distribution is uniform (i.e., $p(\theta) = 1/(2\sqrt{3}\sigma_\theta)$) and that α_ls are circular Gaussian random variables. For fair comparisons between the Uniform and Gaussian spatial distributions, we choose $\sigma = R/3$ to guarantee in the Gaussian distribution case that more than 99% of nodes are located in $D(O, R)$.

Figure 2 plots the empirical ASNRs and ASANRs achieved by $\mathbf{w} \in \{\mathbf{w}_{\mathrm{O}}, \mathbf{w}_{\mathrm{P}}, \mathbf{w}_{\mathrm{M}}\}$ as well as the analytical ASANRs achieved by $\mathbf{w}_{\mathrm{P}}$ and $\mathbf{w}_{\mathrm{M}}$ versus K for $\sigma_\theta = 20$ (deg) and $R/\lambda = 1, 4$. The nodes' spatial distribution is assumed to be Uniform in Fig. 2(a) and Gaussian in Fig. 2(b). From these figures, we confirm that the analytical $\tilde{\xi}_{\mathbf{w}_{\mathrm{P}}}$ and $\tilde{\xi}_{\mathbf{w}_{\mathrm{M}}}$ match perfectly their empirical counterparts. As can be observed from these figures, the proposed DCB outperforms M-DCB in terms of achieved ASANR. Furthermore, the ASANR gain achieved using the proposed DCB instead of the latter substantially increases when R/λ grows large. Moreover, from Figs. 2(a) and (b), the achieved ASANR using the proposed LCSI-based DCB fits perfectly with that achieved using NLCSI-based OCB, which is unsuitable for a distributed implementation in WSNs, when K is in the range of 20 while it looses only a fraction of a dB when K is in the range of 5. This proves that the proposed DCB is able to reach optimality when K is large enough. It can be also verified from these figures that $\tilde{\xi}_{\mathbf{w}_{\mathrm{P}}}$ and $\tilde{\xi}_{\mathbf{w}_{\mathrm{B}}}$ perfectly match $\bar{\xi}_{\mathbf{w}_{\mathrm{P}}}$ and $\bar{\xi}_{\mathbf{w}_{\mathrm{M}}}$, respectively, for $K = 20$. All these observations corroborate the theoretical results obtained in Sect. 5.

Figure 3 displays the empirical ASNRs and ASANRs achieved by $\mathbf{w} \in \{\mathbf{w}_{\mathrm{O}}, \mathbf{w}_{\mathrm{BD}}, \mathbf{w}_{\mathrm{P}}, \mathbf{w}_{\mathrm{M}}\}$ as well as the analytical ASANRs achieved by $\mathbf{w}_{\mathrm{P}}$ and $\mathbf{w}_{\mathrm{M}}$ versus the AS for $K = 20$ and $R/\lambda = 1$. It can be observed from this figure that the ASANR achieved by M-DCB decreases with the AS while that achieved by the proposed beamformer remains constant. This corroborates again the theoretical results obtained in Sect. 5. Furthermore, we observe from Fig. 3 that B-DCB achieves the same ASNR as the proposed DCB when the AS is relatively small such as in lightly- to moderately-scattered environments. Nevertheless, in highly-scattered environments where the AS is large (i.e., $\sigma_\theta \geq 20$ deg), the proposed DCB outperforms B-DCB whose performance further deteriorates as σ_θ grows large. This is expected since the two-ray channel approximation made when designing B-DCB is only valid for small σ_θ. Moreover, it can be noticed from Figs. 3(a) and (b), that the ASNR gain achieved using the proposed DCB instead of M-DCB and B-DCB can reach until about 6.5 (dB) and 4 (dB), respectively. From these figures, we also observe that the curves of $\bar{\xi}_{\mathbf{w}_{\mathrm{P}}}$ and $\bar{\xi}_{\mathbf{w}_{\mathrm{O}}}$ are indistinguishable. As pointed out above, this is due to the fact that both OCB and the proposed DCB constantly reach optimality.

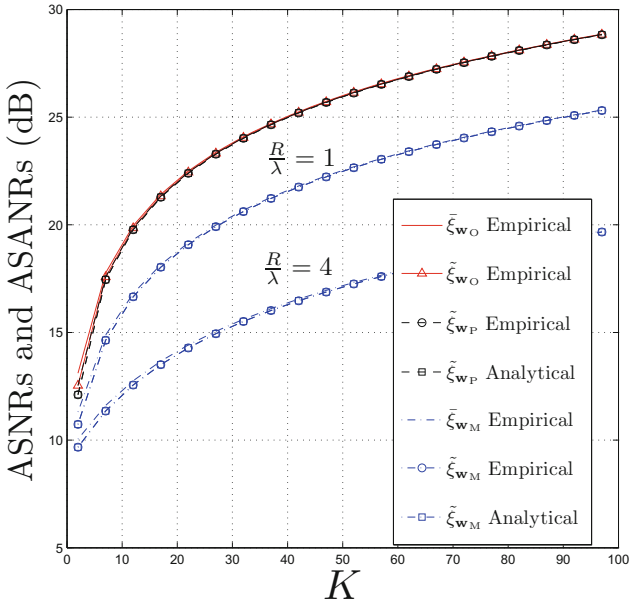

(a) Uniform distribution

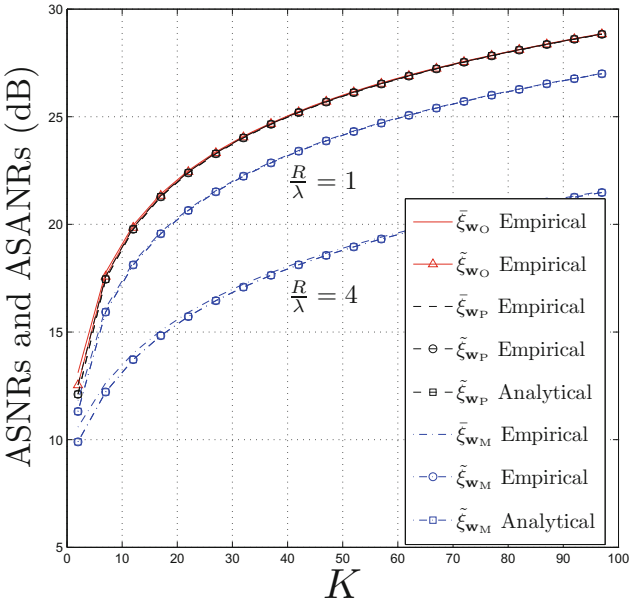

(b) Gaussian distribution

Fig. 2. The empirical ASNRs and ASANRs achieved by $\mathbf{w} \in \{\mathbf{w}_O, \mathbf{w}_P, \mathbf{w}_M\}$ as well as the analytical ASANRs achieved by $\mathbf{w}_P$ and $\mathbf{w}_M$ versus K for $\sigma_\theta = 20$ (deg) and $R/\lambda = 1, 4$ when the nodes' spatial distribution is (a): Uniform and (b): Gaussian.

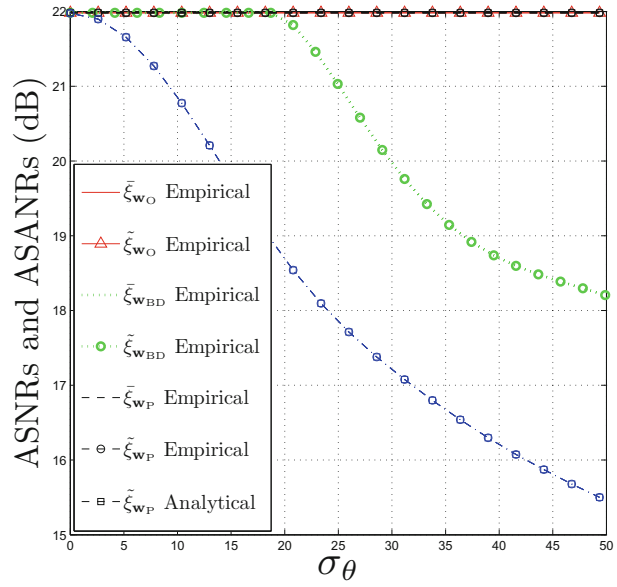

(a) Uniform distribution

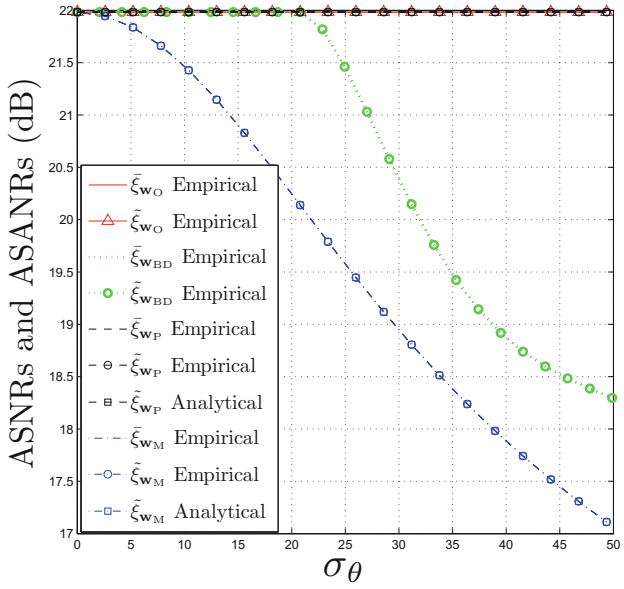

(b) Gaussian distribution

Fig. 3. The empirical ASNRs and ASANRs achieved by $\mathbf{w} \in \{\mathbf{w}_O, \mathbf{w}_{BD}, \mathbf{w}_P, \mathbf{w}_M\}$ as well as the analytical ASANRs achieved by $\mathbf{w}_P$ and $\mathbf{w}_M$ versus σ_θ for $K = 20$ and $R/\lambda = 1$ when the nodes' spatial distribution is (a): Uniform and (b): Gaussian.

7 Conclusion

In this paper, we considered a power-constrained SNR-optimal CB design that achieves a dual-hop communication from a source to a receiver, through a WSN comprised of K independent and autonomous sensor nodes. We verified that the direct implementation of this CB design is NLCSI-based. Exploiting, the polychromatic structure of scattered channels, we proposed a novel LCSI-based DCB implementation that requires a minimum overhead cost and, further, performs nearly as well as its NLCSI-based OCB counterpart. Furthermore, we proved that the proposed DCB implementation always outperforms M-DCB which is designed without accounting for scattering and that it is more robust to scattering than B-DCB whose performance substantially deteriorates in highly-scattered environments.

References

1. Ochiai, H., Mitran, P., Poor, H.V., Tarokh, V.: Collaborative beamforming for distributed wireless ad hoc sensor networks. IEEE Trans. Sign. Process. **53**, 4110–4124 (2005)
2. Ahmed, M.F.A., Vorobyov, S.A.: Collaborative beamforming for wireless sensor networks with Gaussian distributed sensor nodes. IEEE Trans. Wirel. Commun. **8**, 638–643 (2009)
3. Huang, J., Wang, P., Wan, Q.: Collaborative beamforming for wireless sensor networks with arbitrary distributed sensors. IEEE Commun. Lett. **16**, 1118–1120 (2012)
4. Zarifi, K., Ghrayeb, A., Affes, S.: Distributed beamforming for wireless sensor networks with improved graph connectivity and energy efficiency. IEEE Trans. Sign. Process. **58**, 1904–1921 (2010)
5. Ahmed, M.F.A., Vorobyov, S.A.: Sidelobe control in collaborative beamforming via node selection. IEEE Trans. Sign. Process. **58**, 6168–6180 (2010)
6. Mudumbai, R., Barriac, G., Madhow, U.: On the feasibility of distributed beamforming in wireless networks. IEEE Trans. Wirel. Commun. **6**, 1754–1763 (2007)
7. Mudumbai, R., Brown, D.R., Madhow, U., Poor, H.V.: Distributed transmit beamforming: challenges and recent progress. IEEE Commun. Mag. **47**, 102–110 (2009)
8. Han, Z., Poor, H.V.: Lifetime improvement in wireless sensor networks via collaborative beamforming and cooperative transmission. IET Microw. Antennas Propag. **1**, 1103–1110 (2007)
9. Dong, L., Petropulu, A.P., Poor, H.V.: A cross-layer approach to collaborative beamforming for wireless ad hoc networks. IEEE Trans. Sign. Process. **56**, 2981–2993 (2008)
10. Godara, L.C.: Application of antenna arrays to mobile communications, part II: Beam-forming and direction-of-arrival considerations. Proc. IEEE **85**, 1195–1245 (1997)
11. Zarifi, K., Zaidi, S., Affes, S., Ghrayeb, A.: A distributed amplify-and-forward beamforming technique in wireless sensor networks. IEEE Trans. Sign. Process. **59**, 3657–3674 (2011)
12. Zarifi, K., Affes, S., Ghrayeb, A.: Collaborative null-steering beamforming for uniformly distrubuted wireless sensor networks. IEEE Trans. Sign. Process. **58**, 1889–1903 (2010)

13. Astly, D., Ottersten, B.: The effects of local scattering on direction of arrival estimation with MUSIC. IEEE Trans. Sign. Process. **47**, 3220–3234 (1999)
14. Shahbazpanahi, S., Valaee, S., Gershman, A.B.: A covariance fitting approach to parametric localization of multiple incoherently distributed sources. IEEE Trans. Sign. Process. **52**, 592–600 (2004)
15. Souden, M., Affes, S., Benesty, J.: A two-stage approach to estimate the angles of arrival and the angular spreads of locally scattered sources. IEEE Trans. Sign. Process. **56**, 1968–1983 (2008)
16. Bengtsson, M., Ottersten, B.: Low-complexity estimators for distributed sources. IEEE Trans. Sign. Process. **48**, 2185–2194 (2000)
17. Besson, O., Stoica, P., Gershman, A.B.: Simple and accurate direction of arrival estimator in the case of imperfect spatial coherence. IEEE Trans. Sign. Process. **49**, 730–737 (2001)
18. Amar, A.: The effect of local scattering on the gain and beamwidth of a collaborative beampattern for wireless sensor networks. IEEE Trans. Wirel. Commun. **9**, 2730–2736 (2010)
19. Zaidi, S., Affes, S.: Distributed beamforming for wireless sensor networks in local scattering environments. In: Proceedings of IEEE VTC 2012-Fall, Québec City, Canada, 3–6 September (2012)
20. Zaidi, S., Affes, S.: Distributed collaborative beamforming with minimum overhead for local scattering environments. In: Proceedings of IEEE IWCMC 2012, Cyprus, 27–31 August (2012, Invited Paper)
21. Zaidi, S., Affes, S.: Spectrum-efficient distributed collaborative beamforming in the presence of local scattering and interference. In: Proceedings of IEEE GLOBECOM 2012, Anaheim, CA, USA, 3–7 December (2012)
22. Zaidi, S., Affes, S.: Distributed collaborative beamforming in the presence of angular scattering. IEEE Trans. Commun. **62**, 1668–1680 (2014)
23. Zaidi, S., Affes, S.: Distributed collaborative beamforming design for maximized throughput in interfered and scattered environments. IEEE Trans. Commun. **63**, 4905–4919 (2015)
24. Zaidi, S., Affes, S.: SNR and throughput analysis of distributed collaborative beamforming in locally-scattered environments. Wireless Commun. Mobile Comput. **12**, 1620–1633 (2012, Invited Paper). Wiley Journal
25. Zaidi, S., Affes, S.: Analysis of collaborative beamforming designs in real-world environments. In: Proceedings of IEEE WCNC 2013, Shanghai, China, 7–10 April (2013)
26. Havary-Nassab, V., Shahbazpanahi, S., Grami, A., Luo, Z.-Q.: Distributed beamforming for relay networks based on second-order statistics of the channel state information. IEEE Trans. Signal Process. **56**, 4306–4316 (2008)
27. Zaidi, S., Hmidet, B., Affes, S.: Power-constrained distributed implementation of SNR-optimal collaborative beamforming in highly-scattered environments. IEEE Wirel. Commun. Lett. **4**, 457–460 (2015)